fluids

MDPI

Article

Experimental and CFD Investigation of Directional Stability of a Box-Wing Aircraft Concept

Gueraiche Djahid [1,*], Karpovich Elena [1,*], Pikulev Maxim [1], Kuznetsov Alexander [1], Sergey Popov [1] and Manoranjan Sinha [2]

[1] Moscow Aviation Institute, 125993 Moscow, Russia
[2] Department of Aerospace Engineering, Indian Institute of Technology Kharagpur, Kharagpur 721302, West Bengal, India
* Correspondence: d.gueraiche@mai.ru (G.D.); karpovichea@mai.ru (K.E.)

Abstract: This study aimed to explore the directional stability issues of a previously studied light box-wing aircraft model with a pusher propeller engine in the fuselage aft section. Earlier configurations have included the use of fuselage together with a lifting system consisting of two wings joined together at their wingtips with vertical stabilizers. However, these side vertical surfaces failed to provide the aircraft with sufficient directional stability, thus prompting the quest in this study for novel solutions that would exclude the need for a fuselage extension and a typical fin. Solutions included the use of a ducted propeller and few configurations of small "fishtail" vertical fins, which formed part of the aft fuselage itself and coupled with vortex generators on the fuselage surface to improve their interference and heal flow separation at the fuselage aft cone. The results of wind tunnel testing were supported with CFD simulations to explain the flow behavior of each of the studied solutions. Tuft visualization and computed flow patterns allowed identification of the sources of the observed low efficiency in terms of directional stability of the fishtail against a simple idle duct without a propeller. A final configuration with a duct and a modified version of the fuselage fins was achieved that provides enough yaw stability margins for a safe flight.

Keywords: box-wing; tailless; flow visualization; directional stability; yaw moment; tufts

Citation: Djahid, G.; Elena, K.; Maxim, P.; Alexander, K.; Popov, S.; Sinha, M. Experimental and CFD Investigation of Directional Stability of a Box-Wing Aircraft Concept. *Fluids* **2022**, *7*, 340. https://doi.org/10.3390/fluids7110340

Academic Editors: Mehrdad Massoudi and Olga A. Azarova

Received: 16 September 2022
Accepted: 22 October 2022
Published: 27 October 2022

1. Introduction

Despite the long known aerodynamic and structural gains of joint wing configurations in allowing significant wing spans and higher lift-to-drag ratios, due in particular to a lower induced component of drag, only very few prototypes have reached serial production, with most concepts never leaving the drawing board. With the idea of using a second wing for both pitch control and increasing the total lifting surface, a particular operational issue of stability concerns in the yaw channel arises due to the absence of a vertical tail with sufficient lever arm and static moment. Wind tunnel investigations [1–5] have revealed that even vertical surfaces that are large enough at the wing tips and have a total area equivalent to a conventional tail will fail to provide enough moment to ensure directional stability. For this reason, most tandem-wing aircraft are equipped with a conventional vertical fin at the aft fuselage [6–8]. The fin and the unnecessary fuselage length extension lead to a significant wetted area and friction drag penalties, which hinder the induced drag benefits of the concept. Given Prandtl plane concepts are of particular interest for green transport aviation, most recent studies are dedicated to stability issues of large box-wing aircraft concepts [9–13], with extremely few articles about light box-wings. Stephen et al. [14,15] found that stability margins of heavy transport can be improved if the wings have the same area and their spacing is increased. In addition, in terms of stability and flight safety, box-wing concepts have been found to fit regional and smaller aircraft mission profiles rather than larger airliners. Part of the box-plane research project "PARSIFAL", a

comprehensive study by Cipolla et al. [16–18], concluded that static longitudinal stability issues can be leveraged through simultaneous geometrical optimization of both wing sweep angle and spacing, i.e., dihedral as well as the area. However, directional stability details are missing in this concept due to it being equipped with a conventional twin tail with large vertical surfaces that ensures enough stability margin at the cost of a significant wetted area. As can be noted from most recent studies [9–18], longitudinal stability of box-planes has been studied very thoroughly, in particular for heavy transport mission profile at transonic speeds. There is, however, a significant knowledge gap concerning directional stability, especially for a light subsonic box-wing lacking a conventional fin. Taking into account the importance of this issue for flight safety, crosswind landings, spin tendency, and recovery, this topic is urgent. Therefore, this study aimed to fill this gap by providing both experimental and computational data.

In this research, novel concepts were studied in a wind tunnel experiment supplied with CFD flow pictures. These included modifying the shape of the aft fuselage to incorporate vertical "fishtail" fins, along with a ducted pushing propeller, which is already known to be safer and more efficient in generating thrust. The baseline test model was a tailless box-plane design with the wingtips joined with vertical fins. Previous conceptual design and wind tunnel experiments of this box-plane model have investigated the Prandtl plane layout for general aviation applications, confirming both its well-known advantages against an equivalent monoplane and providing solutions to some of its disadvantages [1–5]. This study represents a further development in this research intended to improve the aft fuselage local aerodynamics and solve directional stability issues. Previous experiments have focused on the general aerodynamics of lifting surfaces, fuselage, and the wing fuselage junction areas. This study examined secondary lifting surfaces consisting of a highly nonconventional tail assembly: a ducted fan, different shapes of upper and ventral fishtail fins, combined with few patterns of vortex generators. Even without a propeller, the large "idle" duct was found to generate enough stabilizing yaw moment for directional stability at small sideslips. This effect of the duct was compared to that of vertical stabilizing fishtail surfaces. The shape of these surfaces is designed to minimize the interference drag by integrating their geometry into that of the fuselage aft cone using bioinspired curvilinear shapes tangent to the fuselage line, hence the term "fishtail" (Figure 1). As previous tuft flow experiments have revealed a separation of the aft fuselage cone [4], vortex generators were added in an attempt to sustain an attached flow over the fuselage aft to both reduce its drag and maximize fin efficiency. It was found, however, that the idle duct still provided better directional stability than the combined effect of the vertical fins and vortex generators, probably due to the insufficient area of theses surfaces, which was limited by the ability of the material to withstand air pressure. Taking into account the fact that these are non-airfoiled flat plates with little structural depth and easy to bend under pressure, a few preliminary experiments with trial and error allowed estimation of the maximum feasible area.

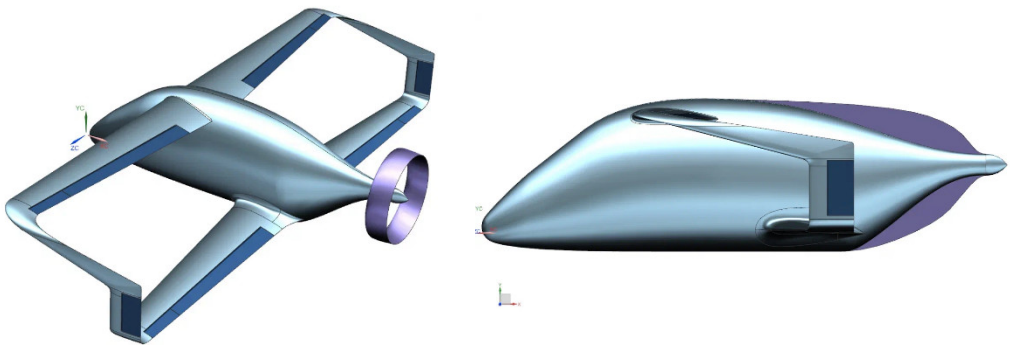

(**a**) (**b**)

Figure 1. Tested configurations of the box-wing model equipped with (**a**) an idle duct and (**b**) vertical fishtail surfaces.

Tuft flow visualization, together with computed pressure and velocity fields near the tail of the studied configurations, revealed insights into the reasons for the low efficiency of the fishtail surfaces, with these fins being strongly influenced by the aft fuselage local flow. The fuselage sidewash was found to significantly reduce the local angle of the attack of the upper fin, while the ventral portion at certain angles of sideslip had a quasi-complete flow separation of the aft cone. Attempts to use wing root fairings, large vortex generators on the fuselage top, and a few patterns of small- and medium-sized VG strakes on the fuselage sides resulted in better flow but insignificant improvements in directional stability. CFD streamlines revealed the size of 3D vortical structures and separation bubbles to be much larger than the vortices from the vortex generators; hence, the model remained unstable. Next, installing the duct allowed the model to gain neutral stability until sideslip angles of ~4°. The duct suffered less interference with the separated aft cone due to its outer section being in much cleaner air and its inner section being much further away from the fuselage surface. Despite that, streamlines, pressure, and velocity fields revealed that the fuselage sidewash caused the inner (shaded) section to experience a significant loss of angle of attack. Beyond sideslip of ~8°, the outer section of the duct separated and lost efficiency as well. Hence, the model remained unstable at sideslips larger than 4–6°. Finally, with the duct providing additional hard points, we investigated attaching to it a pair of large-sized flat plates similar to fishtail fins but with much larger area. With this final configuration of combining the duct and large fins, the model became stable well until large sideslips of ~10°.

It is worth noting that the experiments took place with an idle duct without a propeller. We believe that a rotating pusher propeller would provide enough sucking force to sustain an attached flow on the aft cone, leading to significant efficiency improvement of both the duct itself and the fishtail fins in ensuring more yaw stability. Hence, our current results could be used to validate a dead-stick landing and off-design condition of an idle duct. Future experiments with a rotating propeller might confirm these assumptions. The novelty of this research lies in using multiple nonconventional elements for directional stability of a tailless box-plane layout. These solutions exclude the necessity for a conventional tail fin with an extension of the aft fuselage, hence producing the least possible wetted area and friction drag penalties.

2. Materials and Methods

2.1. Wind Tunnel Experiment

2.1.1. Geometry

To improve the directional stability of the previously studied baseline model of a box-plane aircraft and to investigate innovative ways to boost the yaw channel performance of this aircraft concept, the baseline wind tunnel model was fitted with a duct fixed on 8 thin transversal spokes in the aft-most section of the fuselage, where a future piston engine with a pusher propeller would be installed. Thin spokes were dropped from the CAD model given their effect was neglected (Figure 1a). Another configuration was fitted with flat-plate "fishtail" surfaces tangent to the fuselage lines (Figure 1b), along with vortex generators. Both configurations included tufts for local flow visualization (Figure 2). As the model did not possess a classical tail empennage, yaw control was achieved by rotating rudders located on the vertical fins at the wing tips.

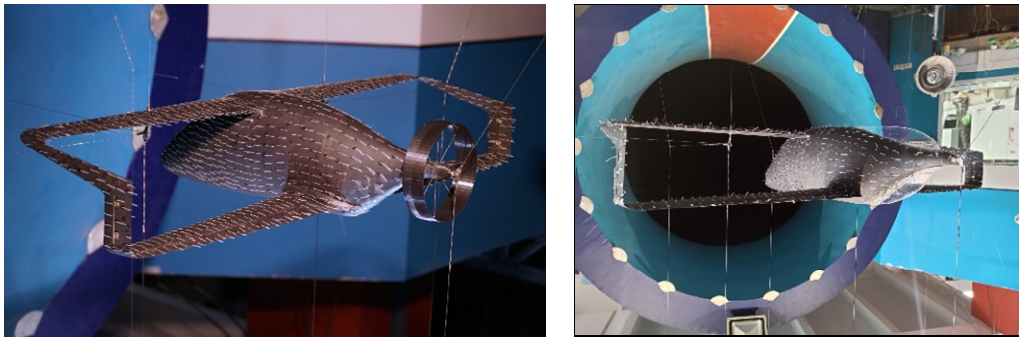

(**a**) (**b**)

Figure 2. Models with tufts for flow visualization in T-1 wind tunnel 2.25 × 3 m test section (**a**) with an idle duct and (**b**) with vertical fishtail surfaces.

Details of the baseline model geometry of the wind tunnel model can be found in [3]. The following main parameters of the wing and fuselage are listed here for reference.

Dimensions (fuselage length × wing span × fuselage height)	0.709 × 1.1 × 0.207 m
Wing aspect ratio	12 (both wings)
Fuselage aspect ratio	3.42
Wing sweep angle at $\frac{1}{4}$ chord	1.6° (fore wing); 3.2° (aft wing)
Airfoil	NACA 3413 (fore wing); NACA 4415 (aft wing)
Airfoil relative thickness	15% (both wings)
Wing incidence angle	2.5° (fore wing); 2° (aft wing)
Elevator-to-wing area ratio	0.17 (both wings)
Flaperon-to-wing area ratio	0.03 (both wings)

Geometry of Fishtail Surfaces

Two configurations of vertical fins were tested. The first was a small version with minimum wetted area, henceforth designated as "S", and fins with a total area of 65.5 cm^2 (Figure 3a). The second had twice the total area, henceforth designated as "L", and fins with a total area 113 cm^2 (Figure 3b). Linear dimensions of both the upper and ventral "L" fins are shown in Figure 4 below.

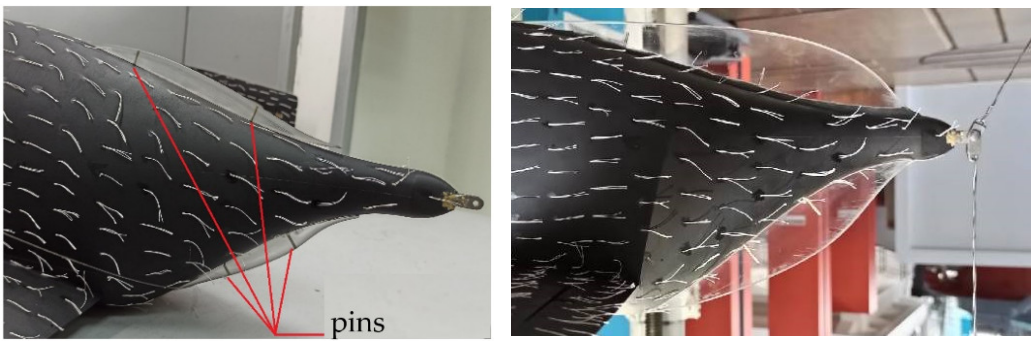

(**a**) (**b**)

Figure 3. Wind tunnel model with tufts and different vertical fins installed to the aft cone with metallic pins: (**a**) small "S" fin configuration; (**b**) large "L" fin configuration.

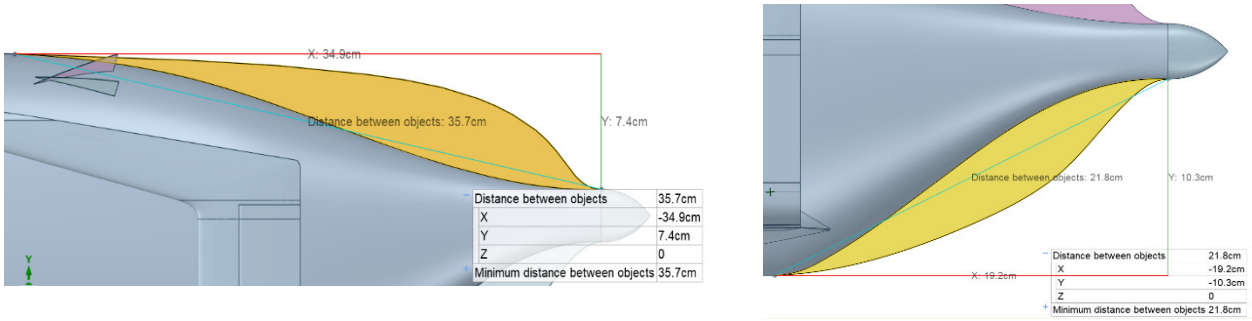

(**a**) (**b**)

Figure 4. Dimensions of the large configuration "L" of vertical fins: (**a**) upper portion of the "L" fin, (**b**) ventral part of the "L" fin.

Geometry of the Duct

Airfoil	NACA0012 (symmetric)
Airfoil thickness	0.5 cm
Duct diameter	17 cm
Hub diameter	3 cm
Spokes	7 × 0.3 cm (8 total)

The duct and its hub were 3D printed from high stiffness plastic; the hub was printed with embedded holes for metallic spoke installation (Figure 5b).

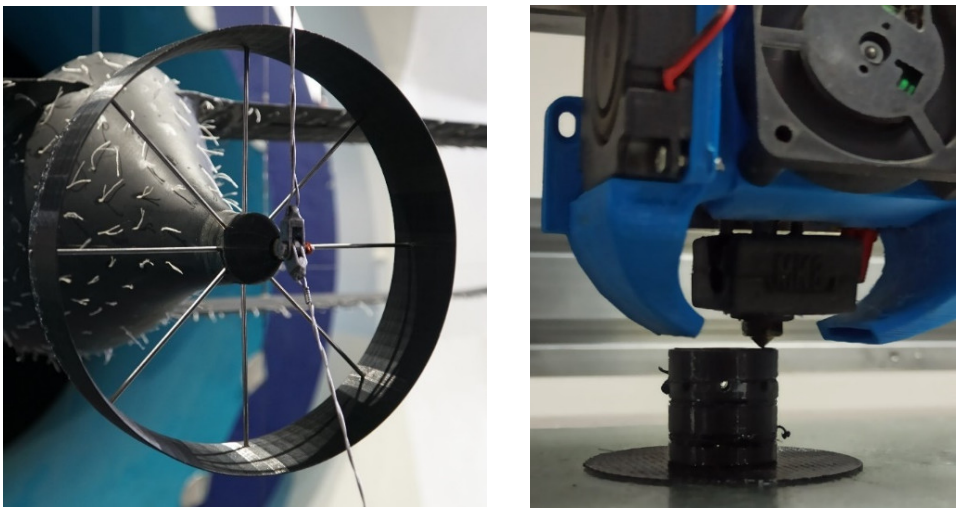

(**a**) (**b**)

Figure 5. (**a**) Aft duct fixed on spokes linked with a hub; (**b**) process of 3D printing of the duct hub.

Vortex Generators

The following problems could be solved using VGs:

- Lateral stability improvement;
- Increasing high-lift devices efficiency.

Suggested positioning:

- Bottom aft fuselage
- Outboard leading edges

Expected outcomes:

- Drag reduction;
- Attached flow on high-lift devices;
- Attached flow on the fuselage aft cone.

Hence, few patterns of small-sized (SVGs), medium-sized (MVGs), and large-sized (LVGs) vortex generators made from tin plate were tested in different locations, and their effect on the fuselage aft cone flow separation as well as on the directional stability were studied.

Table 1 presents the geometrical features of the tested configuration.

Table 1. Geometrical parameters of the tested configurations of vortex generators.

Configuration	Skew Angle δ°	Height h cm	Length l cm	VGs Pitch in a Pattern L cm	Patterns Pitch λ	Min. Distance to Separation Line ΔX_{vg} cm
LVG_1	42	1.1	4.9	4.5	-	-
LVG_2	−42	1.1	4.9	4.5	-	-
MVG_1	35	0.75	1.5	1.5	-	2
MVG_2	35	0.75	1.5	1.5	-	0
MVG_3	−35	0.75	1.5	1.5	-	0
SVG_1	42	0.5	0.75	1	-	6
SVG_2	42	0.5	0.75	1	-	2
Illustration of the geometrical parameters of the vortex generator [19]	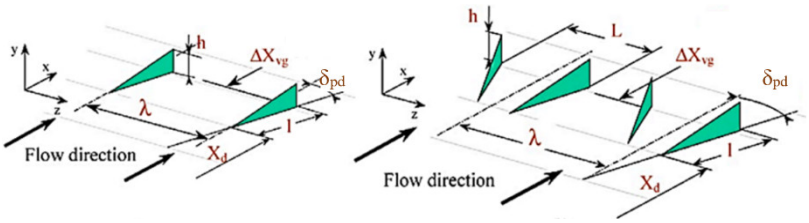					

Large vortex generators (LVGs) were installed on top of the fuselage center-aft section in order to delay separation at high angles of attack. Figure 6 shows the LVGs tested in different positions. In the figure, the converging position is denoted as "1" and the diverging as "2", and the geometrical dimensions of a single VG strake is also given. The LVGs on the wind tunnel test model is given in Figure 7.

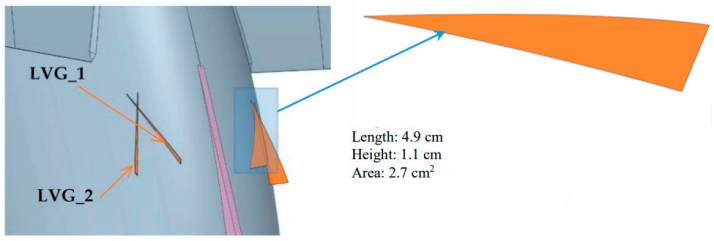

(**a**) (**b**)

Figure 6. (**a**) Large vortex generators (LVGs) in positions 1 (converging) and 2 (diverging); (**b**) single strake geometry and dimensions.

LVG_1 LVG_2

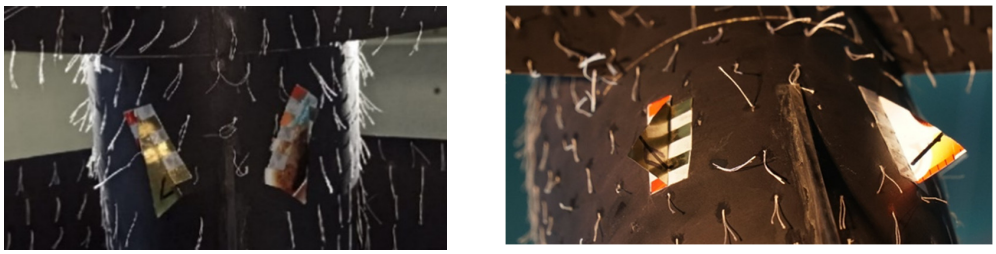

(**a**) (**b**)

Figure 7. Large vortex generators (LVGs) in positions: (**a**) "1" and (**b**) "2" on the wind tunnel model.

Medium-sized vortex generators (MVGs) had the following parameters:

Skew angle δ_{MVG}	~±35°
Pitch L_{MVG}	~1.5 cm
A single MVG strake height	~0.75 cm
A single MVG strake length	~1.5 cm

MVGs were also tested in a few configurations: along a vertical line with a positive β_{MVG}, denoted as MVG_1, and a pattern along an inclined line corresponding to the aft cone separation line with a positive β_{MVG} = +35°, denoted as MVG_2, and with a negative β_{MVG} = −35°, denoted as MVG_3. All configurations on the wind tunnel model are illustrated in Figure 8 below.

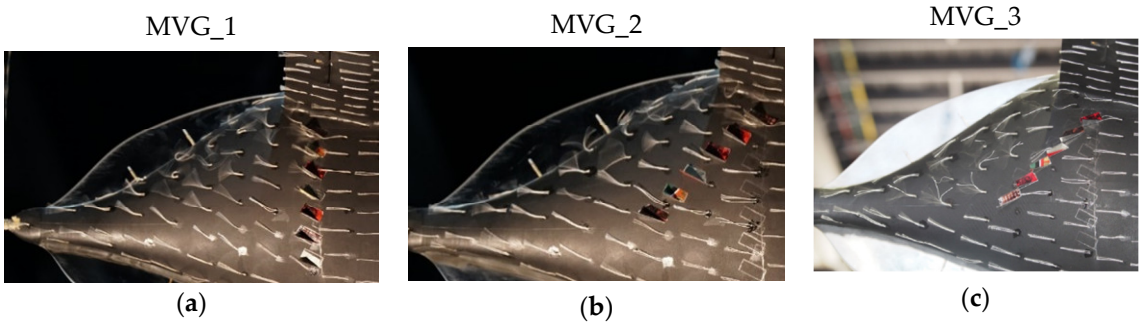

Figure 8. Medium-sized MVG in 3 positions: (**a**) vertical pattern upstream separation line, (**b**) inclined coincident with the separation line, and (**c**) inclined coincident with SL with a negative skew angle.

Small vortex generators (SVGs) had the following geometry:

Skew angle δ_{SVG}	~42°
Pitch L_{SVG}	~1 cm
A single SVG strake height	~0.5 cm
A single SVG strake length	~0.75 cm

Vertical patterns of SVGs were tested in 2 locations: SVG_1, which was close to the aft wing suction peak and well upstream the aft cone separation zone, and SVG_2, which was closer downstream to the separation line (similar to MVG_1), as shown in Figure 9 below.

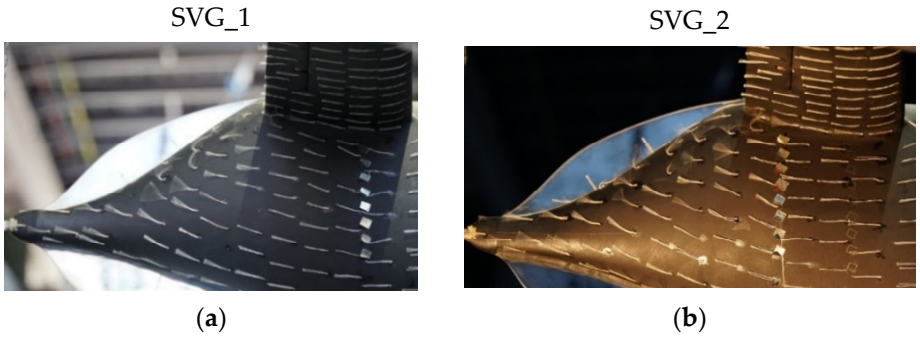

Figure 9. Small SVG in different locations: (**a**) near the aft wing suction peak, (**b**) near the separation line of the fuselage aft cone.

2.1.2. Wind Tunnel Test Conditions

The main geometry and structure of the test model are detailed in [3]. Fine thin silk tufts about 1 cm in length were glued to the surface for local flow observations. The initial tufts axes were coincident with the undisturbed velocity vector or the aircraft *X*-axis. Tests were carried out in wind tunnel T-1 of the Moscow Aviation Institute, which is a subsonic open return circuit type with an open test section. Measurement errors were in the range 3–5%. The main flow parameters at the test section were as follows.

Velocity V∞	38 m/s
Pressure p∞	100,500 Pa
Temperature T∞	293 K
Turbulence intensity ε	0.35%
Reynolds number Re	~10^6
Test section dimensions	Diameter 2.25 m * Length 3.5 m

2.2. CFD Model

2.2.1. Meshing

RANS CFD experiments using ANSYS Fluent were performed on a 30–50 million cells unstructured mesh generated in ANSYS Meshing (Figure 10). For boundary layer resolution, a prismatic layer of 15 layers was built around the wing, fuselage, and additional surfaces (i.e., the duct and fins), as shown in Figure 11. Given the significant impact of the aft fuselage local flow on tail aerodynamics, an extensive automatic refinement algorithm was set as face sizing with a minimum element size of ~10^{-4} m. Based on a similar mesh, the CFD model of the initial configuration was validated against wind tunnel data in [4]. In Figure 12, the wall Y+ function distribution is provided.

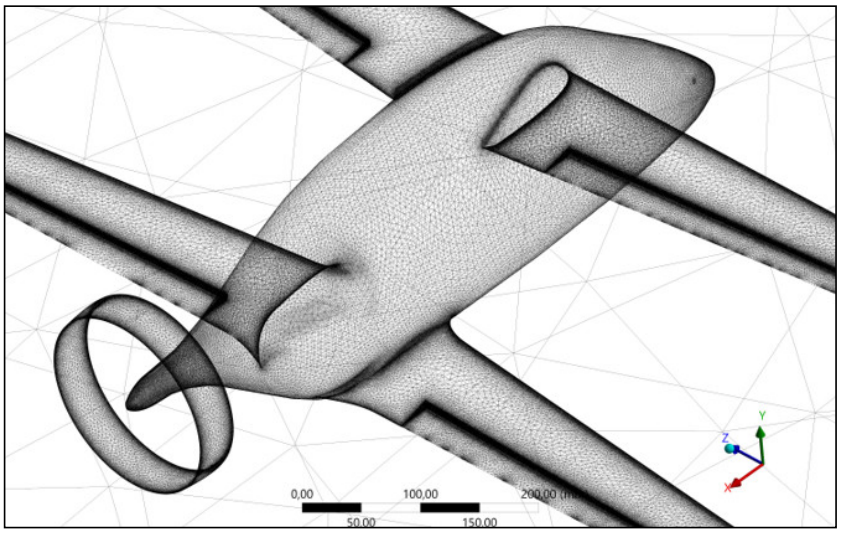

Figure 10. Fragment of the computational mesh of the CFD model with a tail duct.

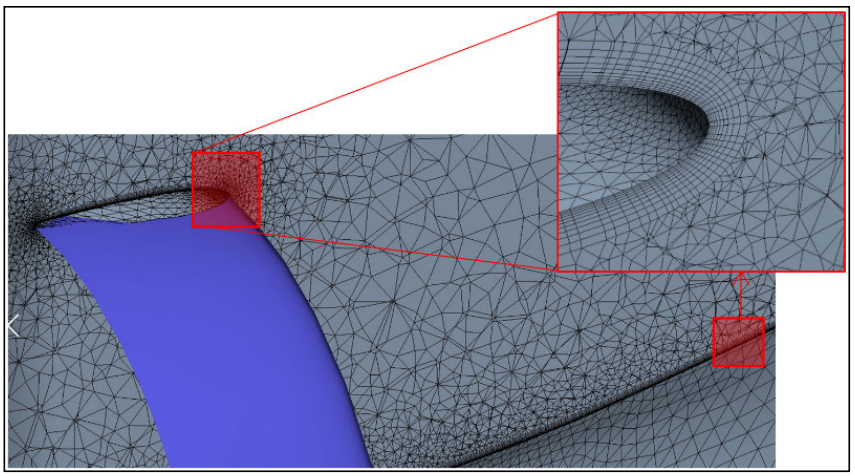

Figure 11. Prismatic boundary layer on both the fuselage and the duct surfaces.

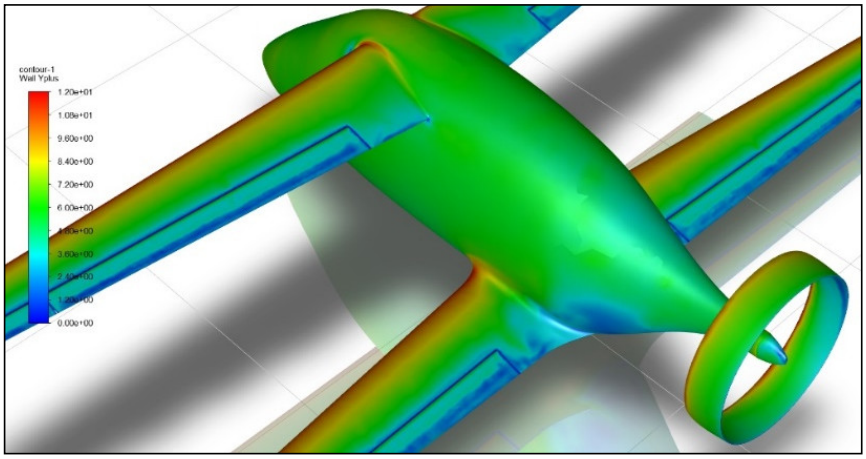

Figure 12. Distribution of wall Y+ values on the CFD model with a duct.

2.2.2. Governing Equations, Discretization Schemes, and Turbulence Modelling

Below are the governing equations solved by the RANS model for an incompressible, low subsonic flow:

Continuity equation:

$$\nabla.(\rho\vec{v}) = 0, \tag{1}$$

Momentum conservation:

$$\nabla.(\rho\vec{v}\vec{v}) = -\nabla p + \nabla.(\bar{\bar{\tau}}). \tag{2}$$

The low subsonic flow (M < 0.3) is incompressible: $\rho = const$; hence, the energy conservation equation was not included in the CFD setup. In addition, as the flow field was incompressible and the temperature was constant (T~293 K), viscosity was treated as a constant value and calculated by the solver based on the chosen fluid material "air": $\mu = const$.

Pressure–velocity coupling was performed through a "coupled" scheme in ANSYS Fluent. For spatial discretization, the Green–Gauss node-based gradient evaluation algorithm was applied; a second-order upwind convective scheme was used for the pressure, density, and momentum. For most of the tested geometry configurations, the solutions converged within 700–1500 iterations.

Turbulence Modelling

Based on the validated initial aircraft configuration [4], the shear stress transport (SST) k-ϖ turbulence model was applied in the current study as well, resulting in good agreement with the wind tunnel experiment of the visualized flow pictures, including the onset prediction and magnitude of the flow-separated areas at the fuselage aft cone (see Table 2 below). The standard k-ϖ model was based on the following transport equations for the turbulence kinetic energy, k:

$$\frac{\partial}{\partial t}(\rho k) + \frac{\partial}{\partial x_i}(\rho k u_i) = \frac{\partial}{\partial x_j}(\Gamma_k \frac{\partial k}{\partial x_j}) + G_k - Y_k \tag{3}$$

and the specific dissipation rate, ϖ:

$$\frac{\partial}{\partial t}(\rho\omega) + \frac{\partial}{\partial x_i}(\rho\omega u_i) = \frac{\partial}{\partial x_j}(\Gamma_\omega \frac{\partial \omega}{\partial x_j}) + G_\omega - Y_\omega \tag{4}$$

Table 2. Computed and tuft-visualized flow field near the aft fuselage and large vertical fins.

β°	4°	7°	9°
Tuft flow visualization	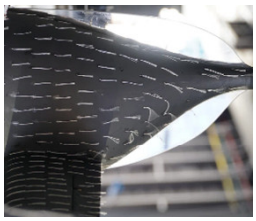	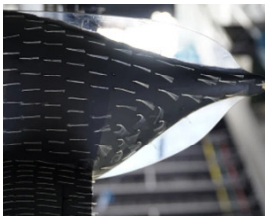	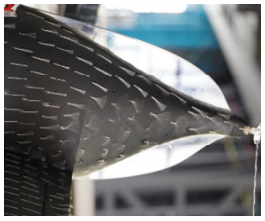
Flow field of the inner (shaded) side of the fuselage	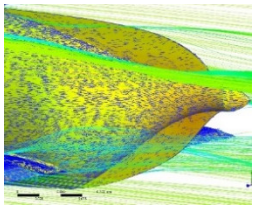	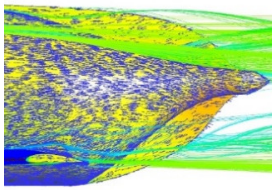	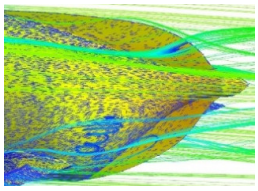
Upper fin Ventral fin	Effective α~β° Weak separation	Effective α < β° partially separated	Effective α < 0 < β° Full separation

Apart from validation purposes, CFD-obtained values of moment coefficients were mostly dropped from the results as the wind tunnel coefficients were enough for the purpose of defining the values of total force and moment coefficients. Instead, CFD experiments were used to supply the wind tunnel data with better details of local and global three-dimensional flow fields, which are hard to achieve in the actual physical experiment.

For validation, the values of the yaw moment coefficient C_n at few points against the wind tunnel data are given in Figure 13. Overall, the model performed well at small angles of sideslip, although it slightly overestimated C_n at negative β. Increasing β led to a similar pattern, leading to greater coefficient misprediction at high α [4], with the CFD model experiencing premature stalling and discrepancy with the experiment at sideslips β~10°. The impact of the fuselage sidewash on directional stability was further revealed in the results and indicated the importance of proper viscosity treatment and Reynolds number. Viscosity was set to a constant based on the wind tunnel Reynolds number and air conditions. As a validation case for the applied SST k-ω turbulence model, we looked at its ability to accurately predict the onset and scale of separation bubbles. Table 2 presents a comparison of the computed flow field and tuft flow visualization.

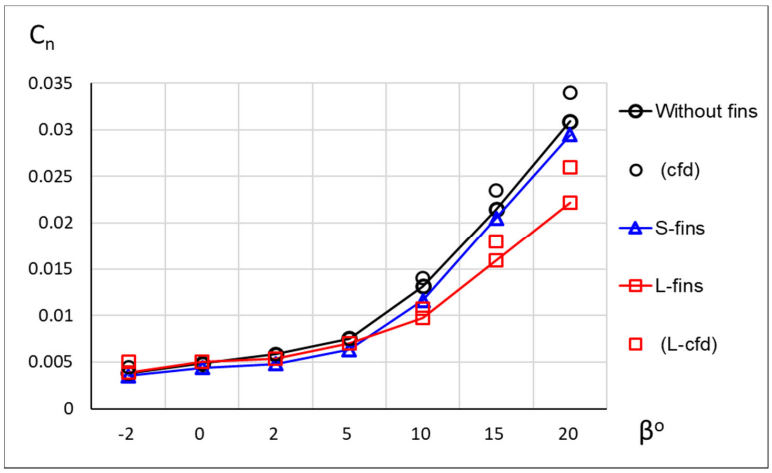

Figure 13. Yaw moment coefficient of the initial model versus the model equipped with small (S) and large (L) vertical fins. Results are provided from both wind tunnel experiment and CFD for validation.

3. Results

3.1. Vertical Fins

As can be seen from the plot in Figure 13, equipping the initial model with vertical fins did not change the overall picture of $C_n(\beta)$ dependency and even with large (L) fins, the model remained unstable in the yaw channel. At small angles of sideslip, both large and small configurations had very little effect on the yaw moment coefficient C_n values. With increasing β, only the large fins gradually started to reduce the yaw derivative. CFD data, which duplicates the wind tunnel values, is given in this plot for validation purpose only. In further results, they were dropped to avoid cluttering the graphs.

An insight into the inefficiency of vertical fins can be gained from the tuft flow visualization and the CFD flow field pictures near the tail at different angles of sideslip (Table 2 and Figure 14). A strong separation of the bottom aft cone at β~9° could be noticed, leading to a 3D vortex upstream the ventral fin and resulting in its virtually complete inefficiency. For the upper fin, the tufts and streamlines showed that it remained attached even at larger β > 9° which is a good sign. However, the computed streamlines showed that its aft-most section received a side-washed flow from the fuselage, reducing its effective angle of attack at moderate β and eventually driving it negative at larger β. Hence, its overall efficiency was strongly affected by interference with the fuselage (see top view of streamlines in Figure 14).

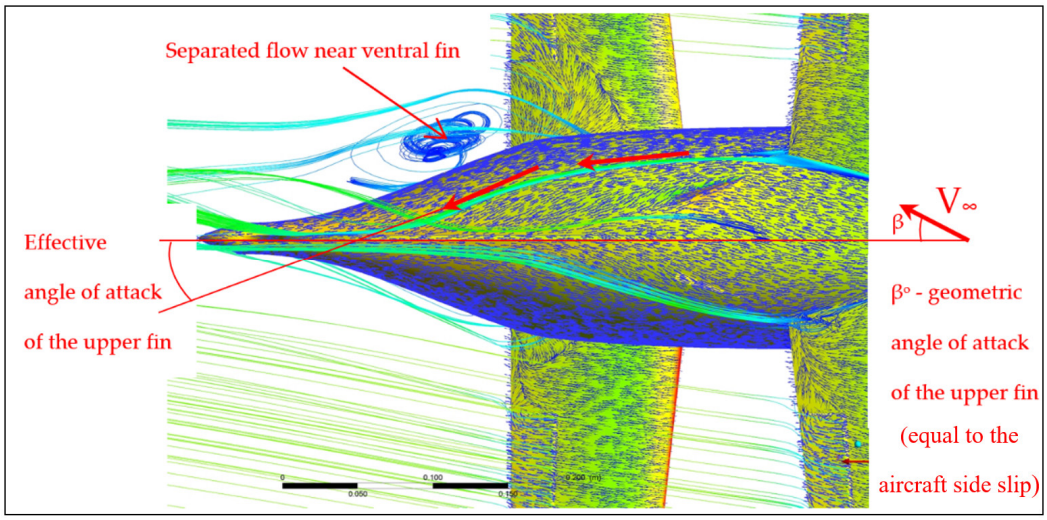

Figure 14. Top view of velocity streamlines at β = +9° revealing a negative effective angle of attack of the upper fin and a 3D vortex near the separated ventral fin.

3.2. Vortex Generators

As has been deduced from the above flow pictures, the main reason for the vertical fin inefficiency can be traced to the boundary flow of the fuselage and its strong influence on the tail fins. Hence, an obvious solution is to use vortex generators to turbulate the flow in problematic areas. First, large LVGs were added to leverage the local effective angle of attack of the upper fin. As mentioned in the Materials and Methods section, we tested both convergent and divergent setting angles of LVG. As can be seen from the plots in Figure 15, the LVG_1 convergent configuration worked slightly better than LVG_2. The geometrical angle of attack of the outer generator, where the upper fin suffered a side-wash, increased as the model sideslip increased, which was probably the reason for the higher vortex intensity. Simultaneously, the inner generator lost the angle of attack with sideslip (see Table 3 below), eventually becoming useless at zero alpha. For LVG_2, this dependency was obviously inverted.

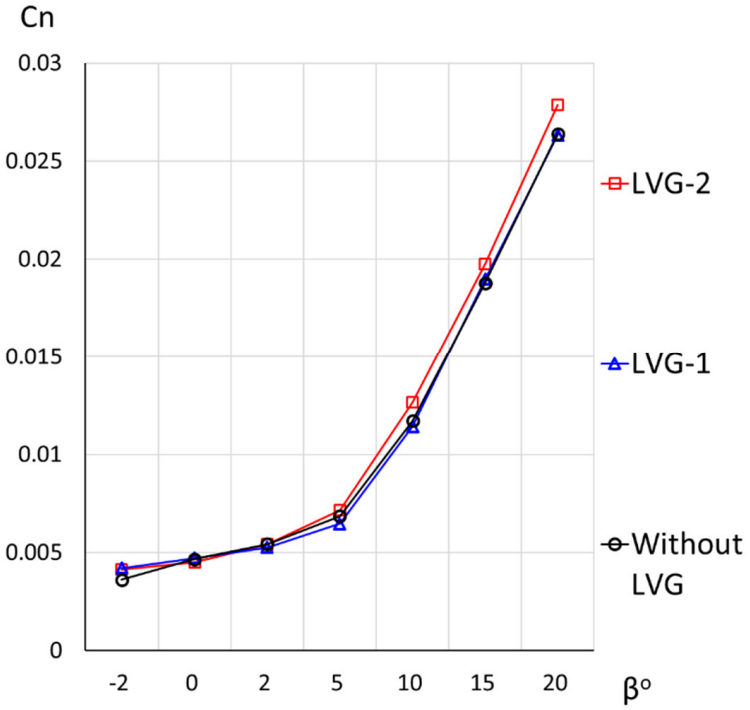

Figure 15. Yaw moment coefficient of the model without vortex generators and with large LVG in positions −1 and −2.

Table 3. Computed flow field near the vortex generators: configuration LVG_1.

β°	3°	7°	15°
Cp scale	-3 -2 -1 -0.6 0.2 1		
	Outer strake		
Top View LVG_1	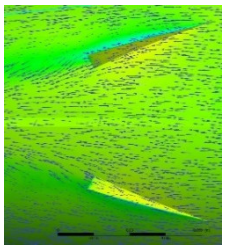	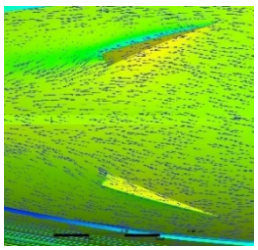	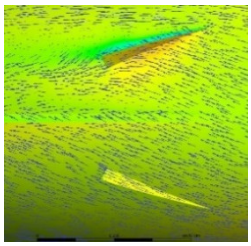
Inner strake Outer strake	Inner strake Moderate—small α Moderate α	Small α High α	α ~ 0 Post-stall α
Outer strake suction side	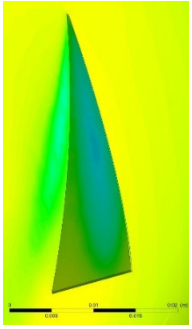	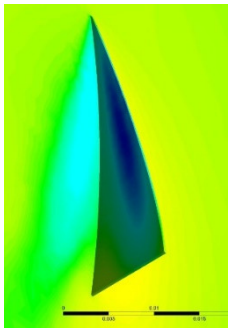	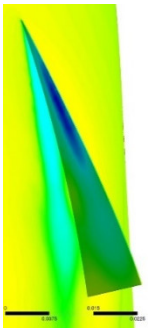
Outer strake remark	Small angle of attack—low vortex intensity	Low pressure covering the entire surface—highest intensity of the vortex.	Low pressure only near the leading edge indicating a stall—overall less vortex intensity

From Table 3 above, we can notice that only the outer VG worked well for the investigated (positive) range of sideslip angles, while the inner one failed to generate a vortex as its (geometric) angle of attack was reduced with sideslip. The geometric α of this inner VG was equal to the VG skew angle (δ, see Table 1) minus the aircraft angle of sideslip. Meanwhile, for the outer VG, sideslip β added to its α, and hence its efficiency increased and reached an optimal at $\beta = 7^{\circ}$. At larger sideslips, a stall led to reduction of the overall vortex intensity. From Figure 16 below, we can notice that the fuselage side wash and its effect on the upper fin remained strong but was delayed to a further position downstream, and hence a smaller portion of the upper fin experienced a negative sidewash. Further moving the LVGs downstream could result in an even less sidewash and better tail efficiency.

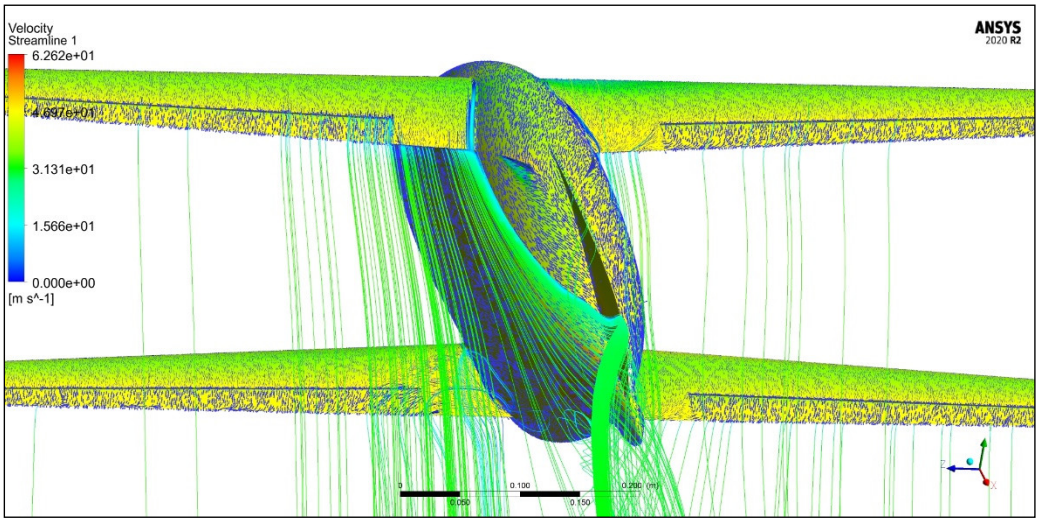

Figure 16. Velocity streamlines on model with LVG_1 and upper fin at $\beta = 15^{\circ}$ showing the fuselage sidewash effect on the upper fin.

Next, in an attempt to improve the ventral fin efficiency by reducing separation of the bottom aft cone, small vortex generators (SVGs) were installed along the side perimeter of the fuselage near the aft wing. Given that separation happens on both the inner and outer sides of the aft cone (Figure 17), VGs were installed on both sides.

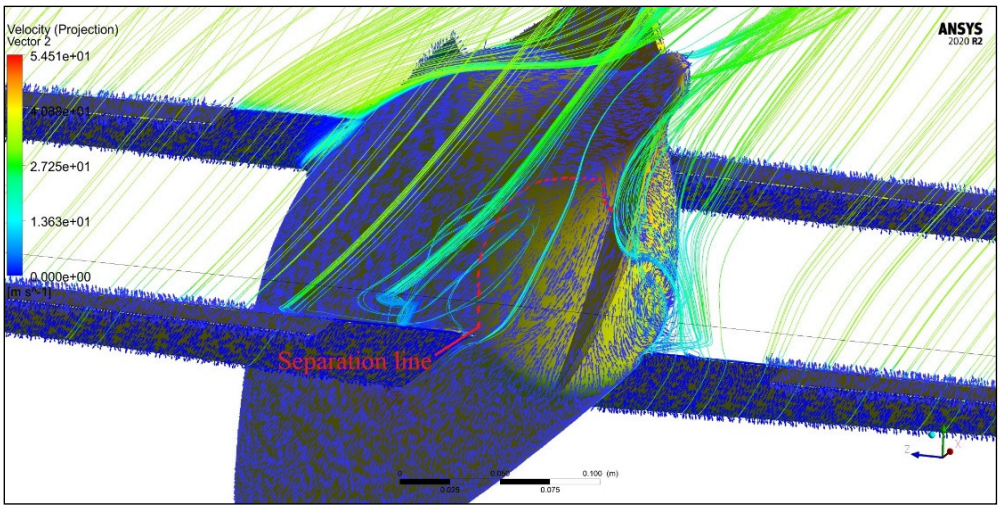

Figure 17. Flow field near the fuselage aft cone.

However, the tuft flow visualization provided in Table 4 revealed that even placing the SVG pattern immediately close upstream to the separation line (version SVG_2) resulted in little improvement of the separated aft cone area, probably due to the 3D vortex structure

taking place (Figure 14) being much larger than vortices generated by the SVGs, hence dominating their local flow. With regard to the investigated velocities of ~37–40 m/s, SVGs were next replaced by medium-sized vortex generators (MVGs).

Table 4. Tuft visualization of the aft fuselage with small VG installed in configurations 1 and 2.

Configuration	L-Fins + LVG	L-Fins + LVG + SVG_1	L-Fins + LVG + SVG_2
Tuft visualization at $\alpha = 2^\circ$	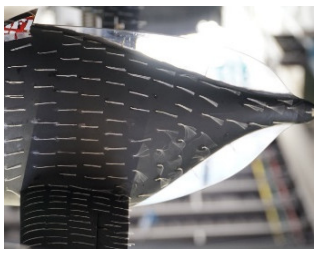		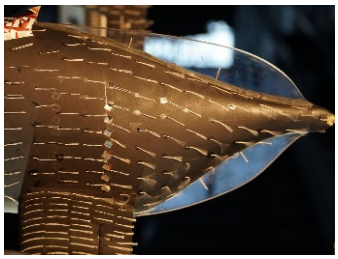
Remarks	Both SVG configurations did not lead to significant reduction of the aft cone separated area. Placing the VG pattern closer downstream led to a slight shift of separation below.		

MVG provided slightly better results in both reducing the separated area size and shifting it further downstream (Table 5). The best effect was achieved by placing an inclined pattern (MVG_2), coincident with the separation line, which is visible in Figure 17. Inverting the strakes (MVG_3) did not give better results, indicating that at the original position, MVG_2 strakes were at a much better angle of attack and generated higher vorticities. However, analysis of the impact of different configurations of MVGs on directional stability, as illustrated by the plots in Figure 18, showed that a good stability increment was achieved by equipping the model with a vertical pattern MVG_1. This could be explained by the fact that MVG_1 deflected the flow towards the ventral fin (see red arrows in Table 5), while MVG_2 deflected it slightly downward towards the separated area itself, giving more attached flow but having less direct effect on the ventral fin. MVG_3 gave the worst results both in terms of separation and stability as the flow was deflected upwards instead. A solution to flow deflection issues could be alternating inverted and positive strakes; however, in view of the increased drag coefficient caused by medium-sized VGs (plot in Figure 19) and their overall insignificant effect on directional stability, we decided to remove them in further experiments. For reducing drag, wing root fairings were added, and their effect was investigated in the subsequent item.

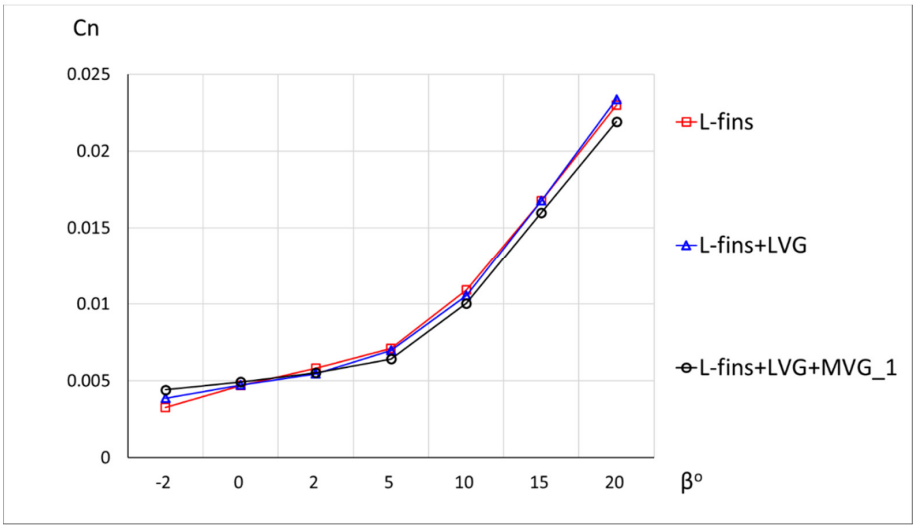

Figure 18. Yaw moment coefficient of the model equipped with combinations of L-fins, LVG, and MVG_1.

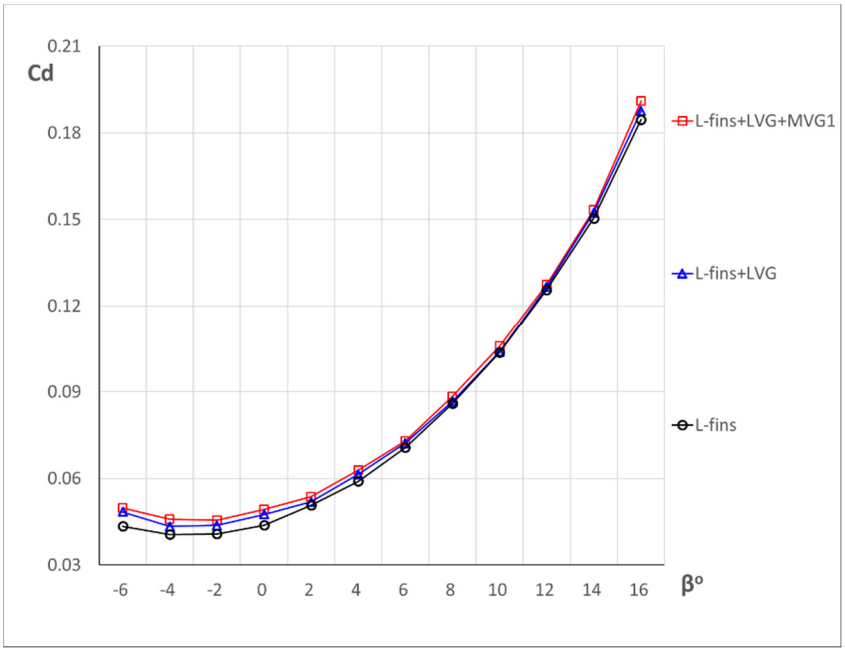

Figure 19. Drag coefficient (Cd) of the model equipped with combinations of L-fins, LVG, and MVG_1.

Table 5. Aft fuselage tuft flow visualization with medium VG installed in configurations 1, 2, and 3.

Configuration	L-Fins + LVG	L-Fins + LVG + MVG_1	L-Fins + LVG + MVG_2
Tuft visualization at $\alpha = 2°$	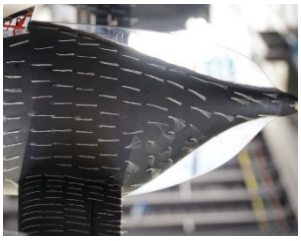	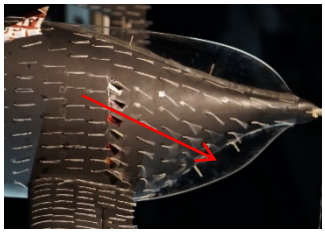	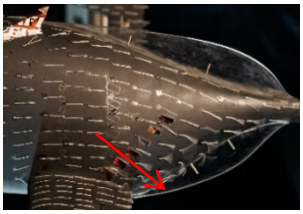
Remarks	• All medium-sized VGs provided a tangible effect on the aft fuselage local flow field. • MVG_2 had the best impact on the separated area as the flow was deflected downward. • MVG_1 provided better directional stability by deflecting the flow towards the ventral fin, thus improving its effect. • Inverting strakes at MVG_3 increased vorticity but led to deflecting the flow upward, exacerbating the aft cone separation and worsening the ventral fin efficiency.		**L-fins + LVG + MVG_3** 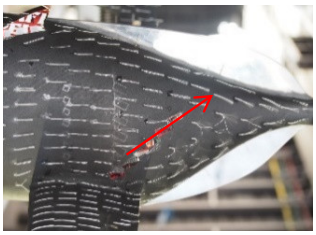

3.3. Wing Root Fairing

Fairings are a common solution to reducing interference drag in junction areas where a discontinuity in the geometry leads to a discontinuity in the flow field, which in turn induces strong pressure gradients, reverse flows, and separation bubbles. As investigated earlier [4], to a large extent, the aft cone separation bubble can be traced to the low pressure at the suction side of the aft wing propagating towards the aft cone and absorbing flow from the higher pressure upper section, causing more reverse flows. Although not directly linked to directional stability, 3D-printed wing root fairings were tested in the current research as a possible quick remedy to aft cone separation in conjunction with other directional stability solutions. As can be seen from the tuft flow visualization at large angles of attack (Table 6), the wing root faring worked as advertised in reducing the extent and intensity of the aft

cone separation bubble. Hence, it was used in further experiments. The fairing impact on directional stability is illustrated in Figure 20. A slight improvement at small to moderate α in the lift/drag ratio of the model is visible in Figure 21. The little improvements in L/D can be explained by the increase in friction drag due to poor surface finishing of the fairing and overall increase in the wetted area.

Table 6. Aft fuselage tuft flow visualization with wing root fairing.

Configuration	Without Wing Root Fairing	Wing Root Fairing Installed
Tuft flow Visualization at $\alpha = 8^{\circ}$		

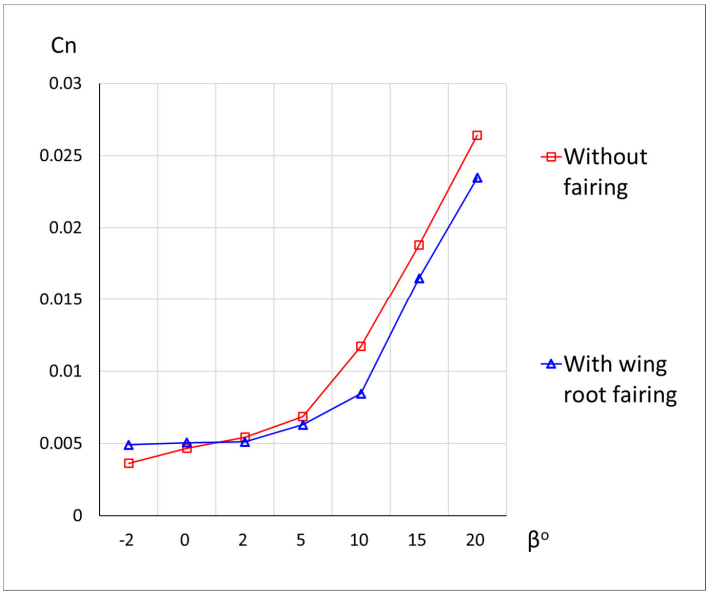

Figure 20. Yaw moment coefficient of the model with and without wing root fairing.

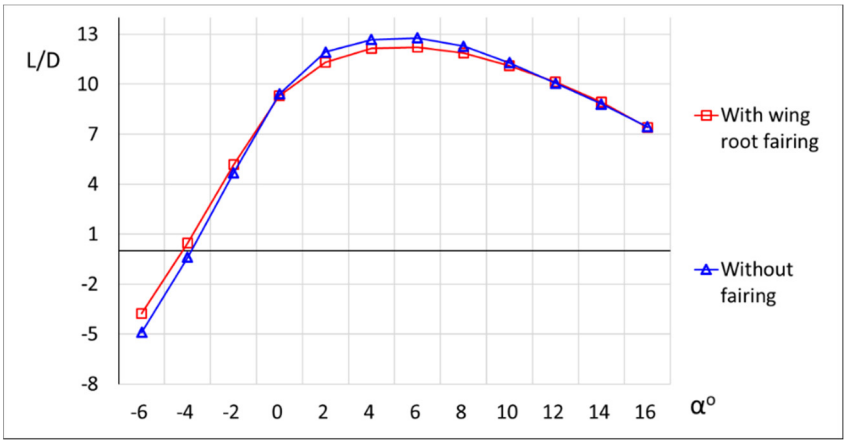

Figure 21. Lift/drag ratio of the model with and without wing root fairing.

3.4. Tail Duct

The above studied combinations of localized solutions did not provide enough directional stability nor completely healed the aft cone separation bubble, which is virtually impossible without globally changing the aft fuselage geometry. Therefore, large vertical surfaces that are far enough from the boundary flow are inevitable for achieving enough directional stability for a safe flight. Instead of a typical vertical fin with large wetted area, we investigated the effect of a ducted fan, which might simultaneously improve the propeller performance and generate enough yaw static moment, especially at significant sideslips. Experiments at the current stage were performed without a propeller. This helped assess directional stability margins of the model in an engine failure mode.

The results of yaw channel coefficient are given in Figure 22 below. The model was stable until angles of sideslip β~2° and then remained neutral until β~5°. This is a relatively much better result compared to vertical fins (Section 3.1). Still, a range of 2–5° of sideslip is too small for flight safety, and hence tuft and CFD flow visualizations were again used to analyze the local flow near the duct for any potential improvements. Streamlines over the model showed that the duct inner side was partially under the influence of the fuselage sidewash and less severe compared to the fin given the duct was at a fairly good distance away from the fuselage, but the local effective angle of attack of the inner shaded side of the duct was significantly reduced (see Figure 23 and Table 7 below).

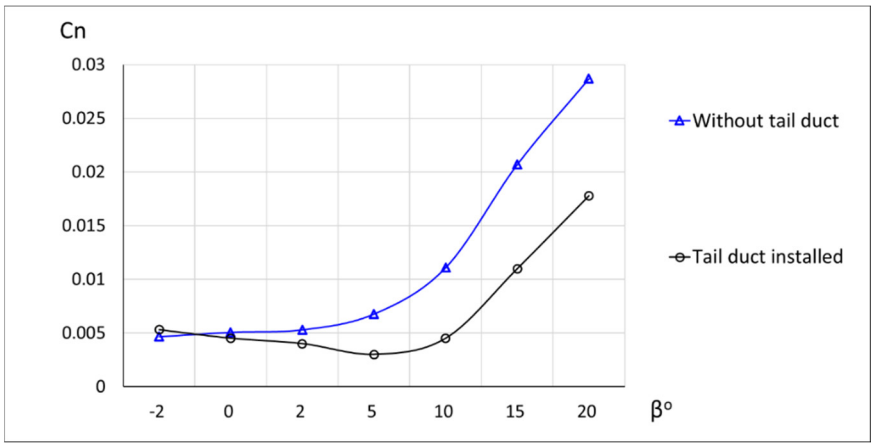

Figure 22. Yaw moment coefficient of the model equipped with a tail duct against the model without a duct.

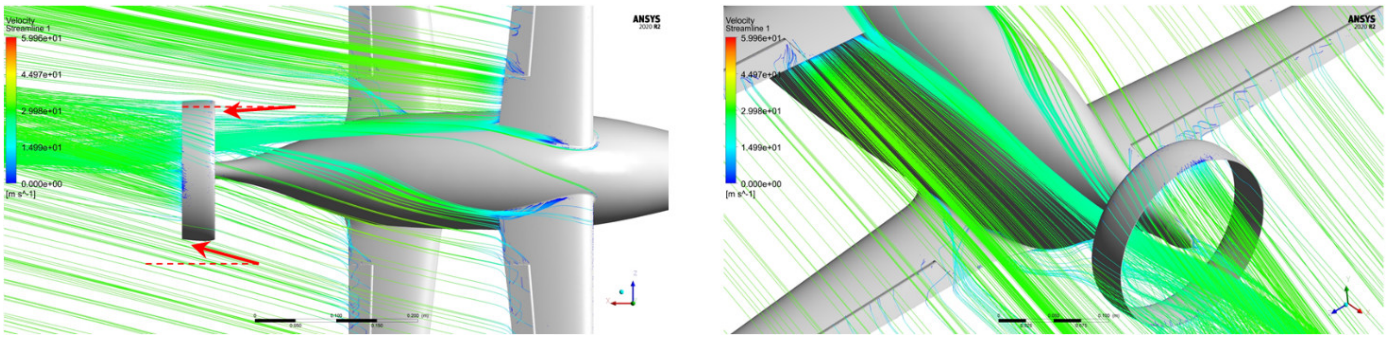

Figure 23. Velocity streamlines at a high sideslip β~15° revealing the impact of the fuselage sidewash on the tail duct inner (shaded) side local effective angle of attack.

Table 7. Pressure field of the tail duct in a horizontal section plane.

β°	3°	7°	15°
Cp scale			
Pressure coefficient visualization in a horizontal mid-section plane	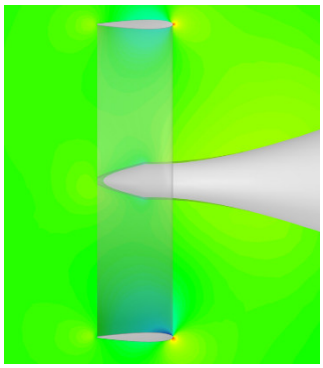	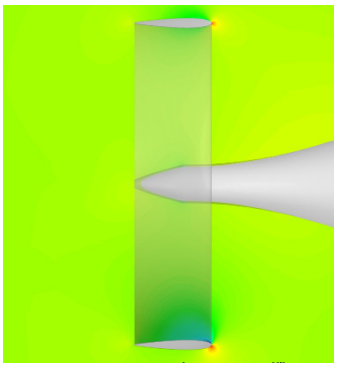	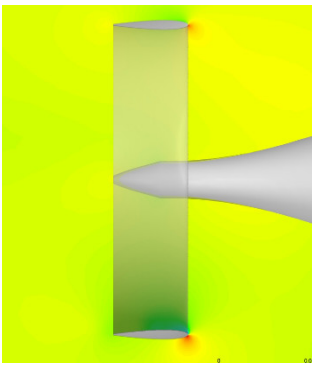
Inner (shaded) section	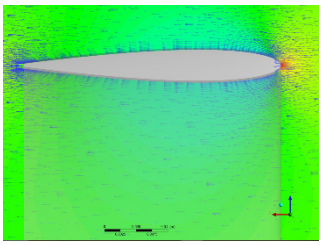	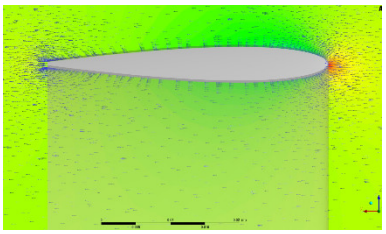	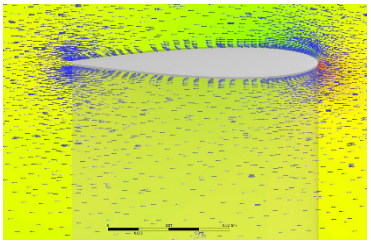
Flow Local effective α	Attached α ~ 0 (symmetric pressure field)	Attached α ~ 0 (symmetric pressure field)	Attached moderate α
Outer section	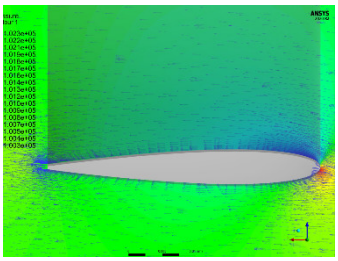	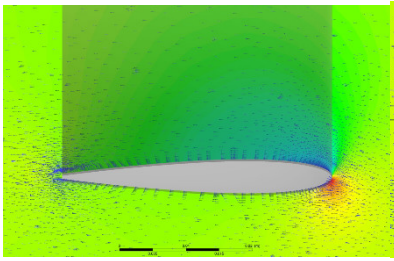	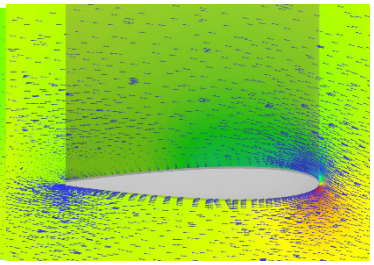
Flow	Attached	Partially separated	Fully separated
Local effective α	Moderate α ~ β ~ 3°	High α ~ β ~ 7°	Extremely high local effective angle of attack α ~ β ~ 15°
Conclusion	The outer section, which was outside the fuselage influence, had an effective α equal to the aircraft (undisturbed) sideslip angle β. The inner section, which was shaded by the fuselage sidewash, experienced a significant loss of effective α, which consequently did not increase with increasing β and hence did not contribute to generating a yaw moment.		

3.5. Final Configuration: Tail Duct Supplied with Large Fins

In view of the good results demonstrated by the tail duct regarding directional stability, at least at small sideslip angles, we decided to keep it for further experiments and to boost its performance with an enlarged version of the earlier studied (Section 3.1) vertical fishtail fins. Unlike the fins in the previous case, which had a small area limited by the ability of the flat plate material to withstand air pressure, this time, the presence of the duct gave us an additional hard point for attaching much larger fins. Supported with three points (Figure 24 below), even a flat zinc plate half a millimeter in thickness was able to withstand significant air pressure at high angles of sideslip.

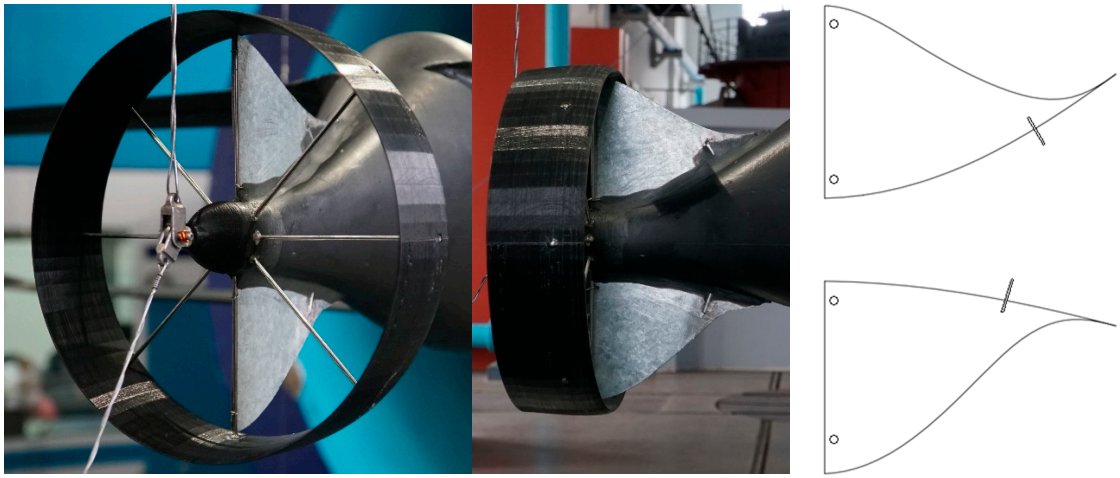

(**a**) (**b**)

Figure 24. (**a**) Wind tunnel model of the final configuration with a tail duct and vertical fishtail fins with a large surface attached to it. (**b**) Attachment was through a 1.7 mm pin inserted in the fuselage and through metal wires tied to the vertical duct metallic spokes.

The results of the model directional stability are plotted below in Figure 25. As can be seen from the plot, the model in this final configuration became stable in the yaw channel well into sideslips of 6–8° and remained neutral beyond 10°. Future wind tunnel and computational experiments with a rotating propeller might reveal the extent of interference and mutual influence between the fins and the propeller, potentially leading to further geometrical optimization of the fins. On the actual aircraft, thicker airfoiled vertical fins might serve to attach the duct to the fuselage, along with similar horizontal surfaces, thus boosting the longitudinal stability performance.

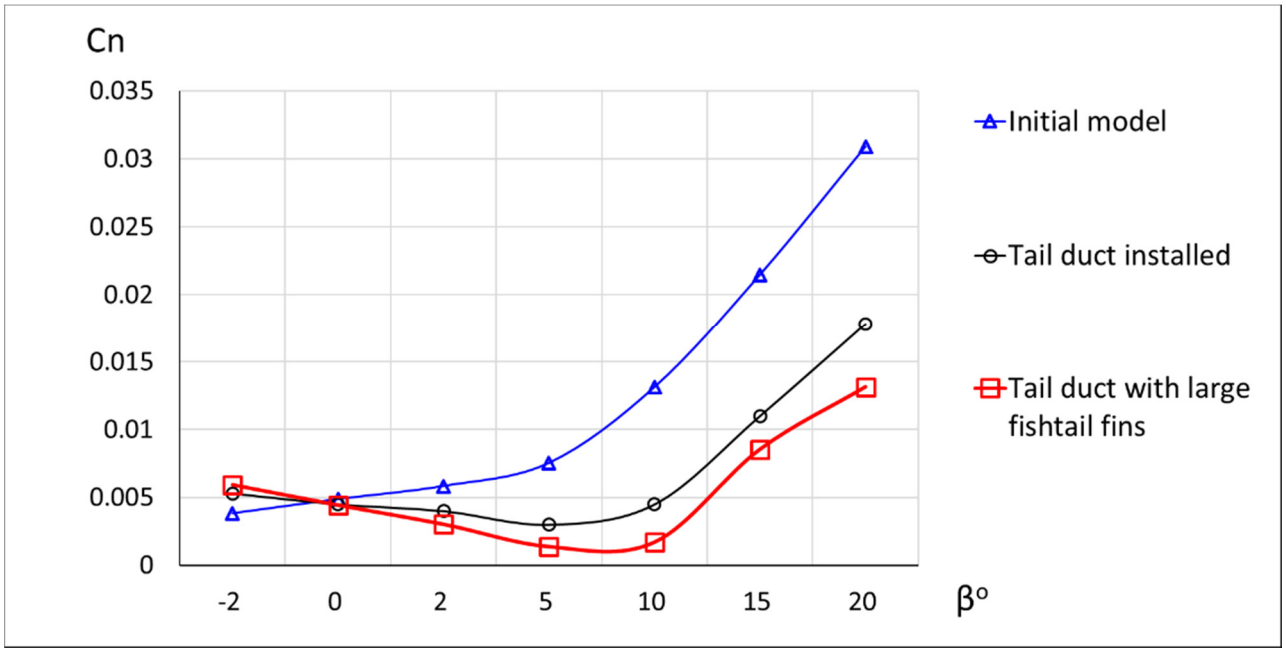

Figure 25. Yaw moment coefficient of the initial model without any additional elements against the model equipped with a tail duct and tail duct supplied with large vertical fins.

4. Discussion and Conclusions

This study experimentally and computationally investigated a tailless nonconventional box-wing aircraft concept with potential applications in general aviation, such as personal

recreational planes, aerotaxis, UAV delivery, etc. An important issue that lies in the way of certification of such flying vehicles is their limited margin of both longitudinal and directional stability. This is a natural consequence of the core idea of the concept to get rid of conventional tails. Multiple studies in the past decades have focused on ways to tackle longitudinal stability, which is easy to achieve by carefully locating the aircraft center of mass and/or ensuring enough spacing of wings. Directional stability, however, is much more challenging in view of an extremely short fuselage. Given the studied concept has a pusher propeller in the tail, it is virtually impossible to locate a vertical fin that is far enough from the center of mass. In addition, extending the fuselage aft section to accommodate a conventional tail would result in significant wetted area and shift the fuselage mass further backwards, which would in effect reduce the lever arm by shifting the aircraft center of mass Hence, in this study, we investigated novel ways to solve this issue while keeping the fuselage geometry intact. A ducted fan and vertical fishtail fins were applied, which were tailored to fit inside the space between the duct and the aft fuselage cone.

The novelty of this research lies in using multiple nonconventional elements for directional stability of a box-plane layout. This excludes the necessity for a conventional tail fin with an extension of the aft fuselage, hence providing the least possible wetted area or "price" to pay for stability, both in terms of friction drag and structural mass. Among the investigated solutions were bioinspired novel surfaces presenting continuity of the aft fuselage geometry itself, combined with vortex generators to improve their efficiency. In addition, equipping the pushing propeller with an airfoiled duct was found to provide very satisfactory results and solved the issue of directional stability of this aircraft concept. The results of the physical experiments were supported with computed local flow fields of pressure and velocity streamlines. This approach revealed deep insights into local flow directions and effective angles of attack as well as the extent of interference zones between different elements, pointing towards sources of efficiency or inefficiency of different solutions and the potential solution.

Author Contributions: Conceptualization, G.D. and K.E.; Data curation, K.E.; Formal analysis, G.D. and K.E.; Funding acquisition, M.S.; Investigation, G.D., K.E., P.M. and K.A.; Methodology, G.D.; Supervision, K.E. and S.P.; Validation, G.D. and K.E.; Visualization, G.D. and K.E.; Writing—original draft, G.D.; Writing—review & editing, G.D., K.E. and S.P. All authors have read and agreed to the published version of the manuscript.

Funding: This work was financially supported by the Russian Science Foundation under Agreement No. 22-49-02047 from 09.03.2022.

Institutional Review Board Statement: Not applicable.

Informed Consent Statement: Not applicable.

Data Availability Statement: Not applicable.

Conflicts of Interest: The authors declare no conflict of interest.

References

1. Karpovich, E.A.; Liseitsev, N.K. Analytical Evaluation of Box Wing Aircraft Aerodynamic Characteristics at Early Design Stages. *Russ. Aeronaut.* **2019**, *62*, 417–422. [CrossRef]
2. Karpovich, E.; Liseitsev, N. Revisiting the Longitudinal Stability and Balance of a Boxwing Aircraft. In *Aerospace Engineering Bulletin*; Perm National Research Polytechnic University: Perm, Russia, 2019; pp. 29–44. [CrossRef]
3. Karpovich, E.A.; Kochurova, N.I.; Kuznetsov, A.V. Experimental Study of Aerodynamic Characteristics of a Boxplane Wind-Tunnel Model. *Russ. Aeronaut.* **2020**, *63*, 659–668. [CrossRef]
4. Karpovich, E.; Gueraiche, D.; Sergeeva, N.; Kuznetsov, A. Investigation of a Light Boxplane Model Using Tuft Flow Visualization and CFD. *Fluids* **2021**, *6*, 451. [CrossRef]
5. Karpovich, E.; Gueraiche, D.; Korotkov, D.A. A method for conceptual design of a light boxplane. *Aerosp. Syst.* **2022**, *5*, 349–356. [CrossRef]
6. Frediani, A.; Cipolla, V.; Oliviero, F. Design of a prototype of light amphibious PrandtlPlane. In Proceedings of the Florida 56th AIAA/ASCE/AHS/ASC Structures, Structural Dynamics, and Materials Conference, Kissimmee, FL, USA, 5–9 January 2015. [CrossRef]

7. IDINTOS: Light Amphibious PrandtlPlane. Available online: http://www.idintos.eu/eng (accessed on 26 October 2022).
8. RUTAN QUICKIE. Available online: https://web.archive.org/web/20150610213002/http://www.aeroresourcesinc.com/store_/images/classifieds/179-1.pdf (accessed on 26 October 2022).
9. Gagnon, H.; Zingg, D.W. Aerodynamic Optimization Trade Study of a Box-Wing Aircraft Configuration. *J. Aircr.* **2016**, *53*, 1–11. [CrossRef]
10. Andrews, S.; Perez, R. Parametric Study of Box-Wing Aerodynamics for Minimum Drag under Stability and Maneuverability Constraints. In Proceedings of the 33rd AIAA Applied Aerodynamics Conference, Dallas, TX, USA, 22–26 June 2015. [CrossRef]
11. Chau, T.; Zingg, D.W. Aerodynamic Shape Optimization of a Box-Wing Regional Aircraft Based on the Reynolds-Averaged Navier-Stokes Equations. In Proceedings of the 35th AIAA Applied Aerodynamics Conference, Denver, CO, USA, 5–9 June 2017. [CrossRef]
12. Cipolla, V.; Frediani, A.; Abu Salem, K.; Binante, V.; Rizzo, E.; Maganzi, M. Conceptual design of Prandtl Plane transport aircraft and preliminary CFD investigation of transonic flight. In Proceedings of the American Institute of Aeronautics and Astronautics 2018 Aviation Technology, Integration, and Operations Conference, Atlanta, Georgia Aviation Technology, Integration, and Operations Conference, Atlanta, GA, USA, 25–29 June 2018. [CrossRef]
13. Andrews, S.A.; Perez, R.E. Analytic Study of the Conditions Required for Longitudinal Stability of Dual-Wing Aircraft. *Proc. Inst. Mech. Eng. J. Aerosp. Eng.* **2017**, *232*, 958–972. [CrossRef]
14. Stephen, A.A.; Ruben, E.P. Stability and Control Effects on the Design Optimization of a Box-Wing Aircraft. In Proceedings of the 14th AIAA Aviation Technology, Integration, and Operations Conference, Atlanta, GA, USA, 16–20 June 2014. [CrossRef]
15. Stephen, A.A.; Ruben, E.P. Multidisciplinary Analysis of a Box-Wing Aircraft Designed for a Regional-Jet Mission. In Proceedings of the 16th AIAA/ISSMO Multidisciplinary Analysis and Optimization Conference, Dallas, TX, USA, 22–26 June 2015. [CrossRef]
16. Cipolla, V.; Abu Salem, K.; Picchi, S.M.; Vincenzo, B. Preliminary design and performance analysis of a box-wing transport aircraft. In Proceedings of the AIAA Scitech 2020 Forum, Orlando, FL, USA, 6–10 January 2020. [CrossRef]
17. Abu Salem, K.; Binante, V.; Cipolla, V.; Maganzi, M. PARSIFAL Project: A Breakthrough Innovation in Air Transport. *Aerotec. Missili Spaz.* **2018**, *97*, 40–46. [CrossRef]
18. PARSIFAL Project. Available online: https://parsifalproject.eu/ (accessed on 26 October 2022).
19. Godard, G.; Stanislas, M. Control of a decelerating boundary layer. Part 1: Optimization of passive vortex generators. *Aerosp. Sci. Technol.* **2006**, *10*, 181–191. [CrossRef]